Hindawi Publishing Corporation
Advances in Materials Science and Engineering
Volume 2016, Article ID 2618253, 11 pages
http://dx.doi.org/10.1155/2016/2618253

Research Article

Photon Conversion and Radiation Synergism in Eu/Tb Complexes Incorporated Poly Methyl Methacrylate

P. Xiao, J. J. Zhang, Z. Q. Wang, and H. Lin

School of Textile and Material Engineering, Dalian Polytechnic University, Dalian 116034, China

Correspondence should be addressed to J. J. Zhang; zhangjj@dlpu.edu.cn and H. Lin; wjs@dlpu.edu.cn

Received 23 January 2016; Revised 23 March 2016; Accepted 28 March 2016

Academic Editor: Mikhael Bechelany

Green and red emissions in terbium and europium benzoic acids (TBA and EBA) incorporated poly methyl methacrylates (PMMA) are exhibited. Larger intensity parameters Ω_2 (11.13×10^{-20} cm^2) and Ω_4 (13.15×10^{-20} cm^2) of Eu^{3+} indicate a high inversion asymmetrical and strong covalent environment around lanthanide (Ln) ions and maximum emission cross section $\sigma_{\text{em-max}}$ (2.45×10^{-21} cm^2) for the dominant transition $^5D_0 \rightarrow {}^7F_2$ of Eu^{3+} reveals the effective photon conversion capacity in EBA incorporated PMMA. Color variation and fluorescence enhancement are validated to be originated from energy transfer and synergistic effect in TBA/EBA coincorporated PMMA system. The results indicate that Eu and Tb complexes incorporated PMMA with effective photon conversion hold great prospect in increment of lighting quality and enhancement of solar-cell efficiency employed in outer space.

1. Introduction

Dye-sensitized solar cells (DSSCs) have attracted extensive attention as one of the promising alternatives for silicon solar cells [1–4]. However, most of the solar radiation energy in the ultraviolet (UV) and infrared (IR) regions is not utilized since DSSCs have a maximum absorption in visible region, which limits the power conversion efficiency of DSSCs [5]. Hence, developing low-cost and high-efficient technologies evokes a great deal of interest in the past decades [6]. Recently, investigations have been reported on the efficient fluorescence generated in lanthanide (Ln) ions incorporated TiO_2 as photoelectrode, which are deemed to be a new route for high-quality conversion efficiency in DSSCs [7–9]. Ln ions can enhance light harvesting via converting UV and near infrared (NIR) radiation to visible emission, so that the conversion efficiency of solar cells will be improved effectively [10–21].

The luminescence of Ln ions originates from the intra-4f transitions, which are forbidden in principle, resulting in relatively low emission efficiency [22]. An effective approach to increase the luminescent efficiency is that chelating Ln ions with organic ligands, which possess advantages such as long emission lifetimes, narrow bandwidths, and large Stokes shifts [23–34]. Since the Ln organic complexes are poor in thermal performances, mechanical stabilities, and processing properties, incorporating these complexes into organic polymers is an ideal method to make up these shortcomings [35–43]. Poly methyl methacrylate (PMMA) exhibits high transparency in the visible spectral region, excellent weather resistance, and high mechanical strength. Moreover, PMMA contains carbonyl groups along with its carbon chain that can be interacted with Ln complexes [44–50]. These characteristics make it suitable as a host material for lanthanide complex doping.

Here in this work, terbium and europium benzoic acid (TBA and EBA) coincorporated PMMA have been prepared. Green and red fluorescence have been observed in TBA and EBA incorporated PMMA, respectively, and the variation of color coordinates originated from synergistic effect of TBA and EBA have been captured. Spontaneous emission probabilities, fluorescence branching ratios, and emission cross sections of intrinsic transitions of Eu^{3+} in PMMA have been evaluated. Thermogravimetric analysis (TGA) was carried out to give a detailed discussion of thermal property of PMMA after the addition of TBA. The analyses of lanthanide complexes incorporated PMMA reveal a promising application prospect for improving illumination quality of lighting

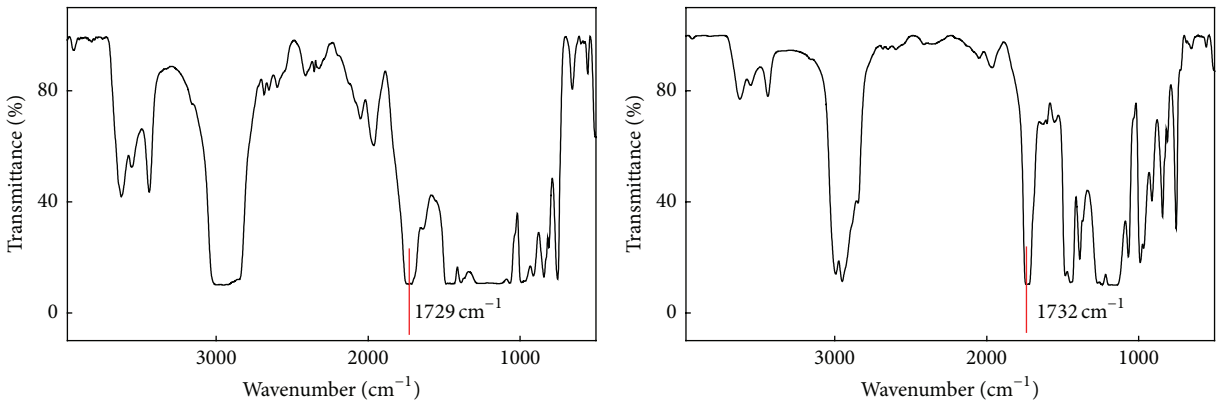

FIGURE 1: FTIR spectra of (a) PMMA and (b) 1 wt% TBA incorporated PMMA.

devices and conversion efficiency of solar cells employed in outer space.

2. Experiments

TBA and EBA were synthesized according to the following procedures. Initially, $LnCl_3$ was synthesized from the reaction between Ln oxides and hydrochloric acid. Then $LnCl_3$ ethanol solution was added dropwise into the benzoic acid (BA) ethanol solution, and the molar ratio of Ln ions to BA was 1 : 3. Subsequently, sodium hydroxide dissolved in ethanol was used to adjust the pH of the mixture to remain between 6 and 7. Instantaneously the precipitate was formed and reaction mixture was stirred adequately for 2 hours at room temperature. The precipitate was filtered off by a Büchner funnel repeatedly, washed with ethanol and water, and dried in an oven at 80°C overnight.

A certain amount of PMMA powder was dissolved in tetrahydrofuran (THF) solution followed by the addition of the lanthanide complexes. The well-mixed solutions were heated at 60°C for 1 hour using a thermostat water bath and the samples were prepared by evaporating the solvent slowly from the solutions.

The infrared spectra of the samples were recorded at room temperature using a Spectrum One-B FTIR spectrophotometer in the range of 400–4000 cm^{-1}. Thermogravimetric analysis scan was carried out by an American TA Company Q-50 thermogravimetric analysis system at a heating rate of 10°C/min under dynamic nitrogen atmosphere with a stream of 50 mL/s. Using the Metricon 2010 prism coupler, the refractive indices of the 0.2 wt% EBA incorporated PMMA were measured to be 1.4870 and 1.4777 at 635.96 and 1536.9 nm, respectively. The refractive indices at other wavelengths can be solved by Cauchy's equation $n = A + B/\lambda^2$ with $A = 1.4758$ and $B = 4526\,\text{nm}^2$. The excitation and emission spectra were recorded by a Hitachi F-7000 fluorescence spectrophotometer and the relative spectral power distributions were measured by a Jobin Yvon Fluorolog-3 spectrophotometer with the calibration of a referenced halogen lamp. The luminescence pictures of the samples were taken using a Sony α200 digital camera.

3. Results and Discussion

Infrared spectroscopy is a useful technique to reflect the supramolecular interaction between the molecules. Taking an example of TBA incorporated PMMA, Fourier transform infrared (FTIR) spectra of pure PMMA and TBA incorporated PMMA in the spectral range 400–4000 cm^{-1} are shown in Figure 1. The peaks at 989 and 1384 cm^{-1} are attributed to C–O–C symmetric stretching and O–CH_3 deformation, respectively, corresponding to fingerprint vibrations of the PMMA [51]. The intense and sharp band at 1729 cm^{-1} for the PMMA corresponds to the (–COOR), which is assigned to symmetrical stretching vibration of the carbonyl group [52]. The asymmetric stretching vibration modes of CH_3 and CH_2 show a strong broad band centered at about 2952 cm^{-1}, indicating a high hydrogen content in the carbon backbone of PMMA [53]. Moreover, new peaks at 1603 and 1554 cm^{-1} appear, corresponding to the asymmetric stretching vibration of COO–, which demonstrates the coordination between the BA and the Ln ions [54].

The IR spectra show that the positions of carbonyl vibration in PMMA and TBA incorporated PMMA are located at 1729 and 1732 cm^{-1}, respectively. The wavenumber difference reveals that the terbium complex is stabilized through chemical interactions with the oxygen atoms of the carbonyl group of PMMA [55], since the oxygen atoms of the carbonyl group in PMMA are a kind of hard base and lanthanide ions are regarded as a kind of hard acid according to HSAB theory [56]. When Tb^{3+} ion interacts with oxygen atom of the carbonyl group, the electron density changes, consequently leading to the position shift corresponding to its characteristic vibration [57].

Thermal property is of great significance to PMMA for practical applications as optical materials and it is strongly influenced by the chain lengths of the polymer, the placements of the ester, and the methyl groups along the polymer backbone [58]. Thermogravimetric analyses (TGA) of PMMA and TBA incorporated PMMA have been carried out to explore their degradation behavior, as illustrated in Figure 2. TGA thermogram of PMMA appears with a maximum value at 143°C on the weight loss rate curve and shows

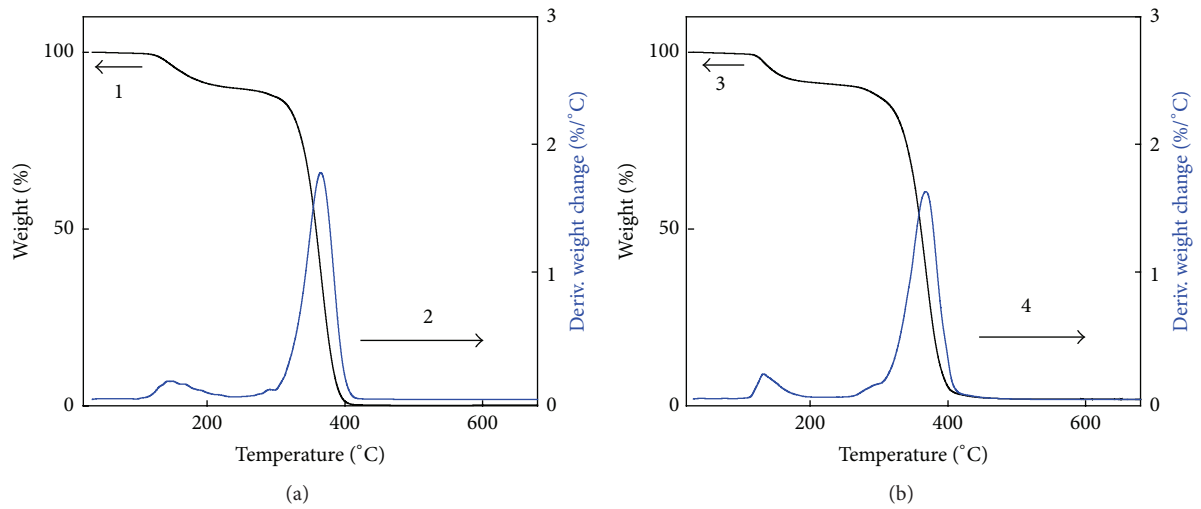

Figure 2: Thermogravimetric analysis of (a) PMMA and (b) 1 wt% TBA incorporated PMMA. Curves 1 and 3 are the weight loss curves, and curves 2 and 4 are the weight loss rate curves.

a 10 wt% total weight loss at 260°C, which is attributed to the solvent removal from the TBA incorporated PMMA. The figure reveals that the major weight loss events that occurred begin at the temperature of 300°C, leaving essentially no residue at 420°C, indicating the thermal decomposition behavior of pure PMMA. In addition, the TGA data show that TBA incorporated PMMA has no weight loss event within 260–330°C due to the water molecules coordinated to the Tb^{3+} ion of the hydrate precursor complex after the doping reaction, and it can be deduced that the TBA framework decomposed and turned into terbium oxide at the temperature of 450°C.

TBA incorporated PMMA emits bright green fluorescence under the radiation of UV lamp as shown in inserted photo of Figure 3. The excitation spectrum of PMMA polymer incorporated with TBA by monitoring the emission at 546 nm is shown as curve 1 in Figure 3. The excitation spectrum is dominated by an intense broad band in the 220–300 nm region, which can be assigned to the absorption of Ln organic complex. The intense band confirms that TBA incorporated PMMA can be efficiently excited under the short-wavelength UV radiation.

Curve 2 in Figure 3 presents the emission spectrum of the PMMA polymer incorporated with TBA under 254 nm excitation. From the emission spectrum, four emission transitions have been identified at 488, 546, 583, and 619 nm, respectively, assigning to the characteristic $^5D_4 \rightarrow {}^7F_J$ (J = 6, 5, 4, 3) transitions within the $4f^8$ configuration of the Tb^{3+} ions [59–61]. The most intense emission peak corresponding to $^5D_4 \rightarrow {}^7F_5$ transition of Tb^{3+} ions is located at 546 nm with a full-width at half-maximum (FWHM) of only 10 nm, and its intensity is apparently stronger than other peaks, resulting in a bright green emission under 254 nm UV radiation. Furthermore, the PMMA matrix influences the coordination environment of Tb^{3+} ions, which causes the change of energy transfer probability from BA to Tb^{3+} and the increase of electric-dipole transition intensity [62].

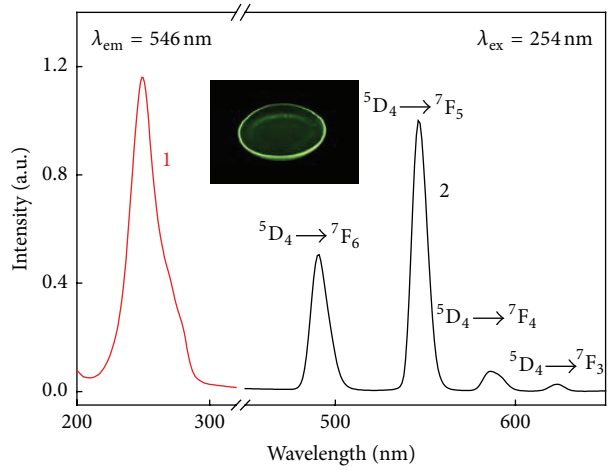

Figure 3: Excitation (curve 1) and emission (curve 2) spectra for 0.2 wt% TBA incorporated PMMA. Inserted photo: fluorescence from TBA incorporated PMMA under 254 nm UV radiation.

Luminescence color for the lanthanide complexes incorporated PMMA is a psychophysical property of human eye and it needs to be expressed mathematically for precision. Thus, marking color coordinates on standard chromaticity diagram is necessary. The Commission International del'Eclairage- (CIE-) 1931 color coordinates can be calculated using the following formula:

$$x = \frac{X}{X+Y+Z},$$
$$y = \frac{Y}{X+Y+Z}, \quad (1)$$
$$z = \frac{Z}{X+Y+Z},$$

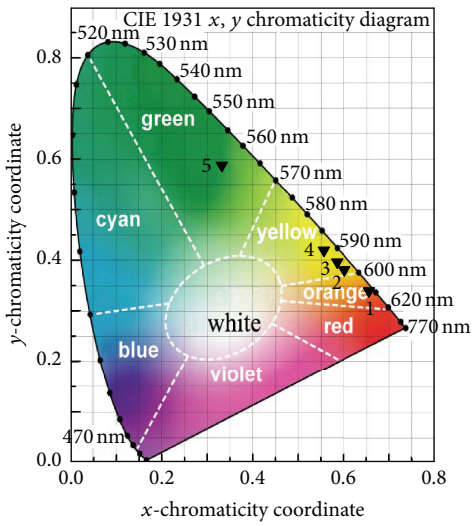

FIGURE 4: CIE (x, y) chromaticity diagram indicating the color coordinates of the fluorescence in samples, and the coordinates corresponding to points from 1 to 5 are in 0.2 wt% EBA, 0.4 wt% TBA-0.2 wt% EBA, 0.8wt% TBA-0.2 wt% EBA, 1.4 wt% TBA-0.2 wt% EBA, and 0.2 wt% TBA incorporated PMMA.

where X, Y, and Z are the three tristimulus values. The tristimulus values for a color can be derived through the relative spectral power distribution $P(\lambda)$ by

$$X = \int P(\lambda)\,\overline{x}(\lambda)\,d\lambda,$$
$$Y = \int P(\lambda)\,\overline{y}(\lambda)\,d\lambda, \quad (2)$$
$$Z = \int P(\lambda)\,\overline{z}(\lambda)\,d\lambda,$$

where λ is the wavelength of the equivalent monochromatic light and $\overline{x}(\lambda)$, $\overline{y}(\lambda)$, and $\overline{z}(\lambda)$ are the three color-matching functions. The values of (x, y) coordinate for TBA incorporated PMMA are calculated to be (0.3327, 0.5877), as point 5 in Figure 4.

The emission spectrum of EBA incorporated PMMA under 254 nm excitation is presented in Figure 5(a), which consists of five emission bands $^5D_0 \rightarrow {}^7F_J$ $(J = 0, 1, 2, 3, 4)$ located at 578, 591, 617, 650, and 698 nm, respectively. Intensity parameters Ω_t $(t = 2, 4, 6)$, which were calculated from the emissions of Eu^{3+}, are important indicators to predict some radiative properties [63, 64]. The integrated fluorescence intensity ratio between the electric-dipole (A_{ed}) and the magnetic-dipole (A_{md}) transitions has been widely used as a criterion of the coordination status and the site asymmetry for the lanthanide ions [65–67], which is calculated based on the emission photon ratio of $^5D_0 \rightarrow {}^7F_J$ $(J = 2, 4, 6)$ transition to $^5D_0 \rightarrow {}^7F_1$ transition, following the formula

$$\frac{A_{md}}{A_{ed}} = \frac{N_J}{N_1}. \quad (3)$$

The transitions of Eu^{3+} from $^5D_0$ to ^7F_J $(J = 2, 4, 6)$ belong to electronic dipole transition and the spontaneous radiative transition probability A_{ed} from ψJ to $\psi' J'$ is described by

$$A_{ed} = \frac{64\pi^4 e^2 \nu^3}{3h(2J+1)} \frac{n\left(n^2+2\right)^2}{9} \sum_{t=2,4,6} \Omega_t \left\langle \psi J \left\| U^{(t)} \right\| \psi' J' \right\rangle^2, \quad (4)$$

where h is the Planck constant, e is the electron charge, n is the refractive index, J is the total angular momentum of the excited state, ν is the wavenumber of transition, Ω_t is the Judd-Ofelt parameters, and the term $\langle \psi J \| U^{(t)} \| \psi' J' \rangle^2$ is the square of the reduced matrix elements. The transition $^5D_0 \rightarrow {}^7F_1$ is a magnetic-dipole transition and the spontaneous transition probability A_{md} is reduced by

$$A_{md} = \frac{64\pi^4 \nu^3}{3h(2J+1)} n^3 S_{md}, \quad (5)$$

where S_{md} is the magnetic-dipole line strength, which is a constant and independent of the medium, so the value of A_{md} can be estimated by the value of fluoride glass $(A'_{md} = 60.3\ s^{-1})$. The relationship is

$$A_{md} = \left(\frac{n}{n'}\right)^3 A'_{md}, \quad (6)$$

where $n'(= 1.522)$ is the refractive index of fluoride glasses [68].

Based on the relative spectral power distribution $P(\lambda)$ of the EBA incorporated PMMA, which is shown in Figure 6(a), the relative photon distribution $N(\nu)$ has been derived as

$$N(\nu) = \frac{\lambda^3}{hc} P(\lambda), \quad (7)$$

where λ is the wavelength, h is the Planck constant, and c is the velocity of light. The relative photon distribution was presented in Figure 6(b), and the emitted photon numbers were calculated using the Gaussian multipeaks fitting and listed in Table 1.

Due to the selection rules and the characteristics of transition intensities in Eu^{3+} ions, each of the $\langle \psi J \| U^{(t)} \| \psi' J' \rangle^2$ parameters determines the intensities of the transitions since the remaining two are zero [69]. The intensity parameters Ω_t $(t = 2, 4)$ of EBA incorporated PMMA were calculated to be 11.13×10^{-20} and 13.15×10^{-20} cm^2, respectively. The value of Ω_6 was not obtained due to the absence of $^5D_0 \rightarrow {}^7F_6$ transition emission. The value of Ω_2 and Ω_4 reflects large chemical bond overlap polarizability to some degree, indicating a high inversion asymmetrical and strong covalent environment around Eu^{3+} in PMMA [67].

The spectroscopic parameters including spontaneous emission probabilities of electric-dipole transition A_{ed} and magnetic-dipole transition A_{md}, total transition probability A_T, fluorescence branching ratios β, and radiative lifetime τ_{rad} are calculated by Ω_t values and listed in Table 2. The

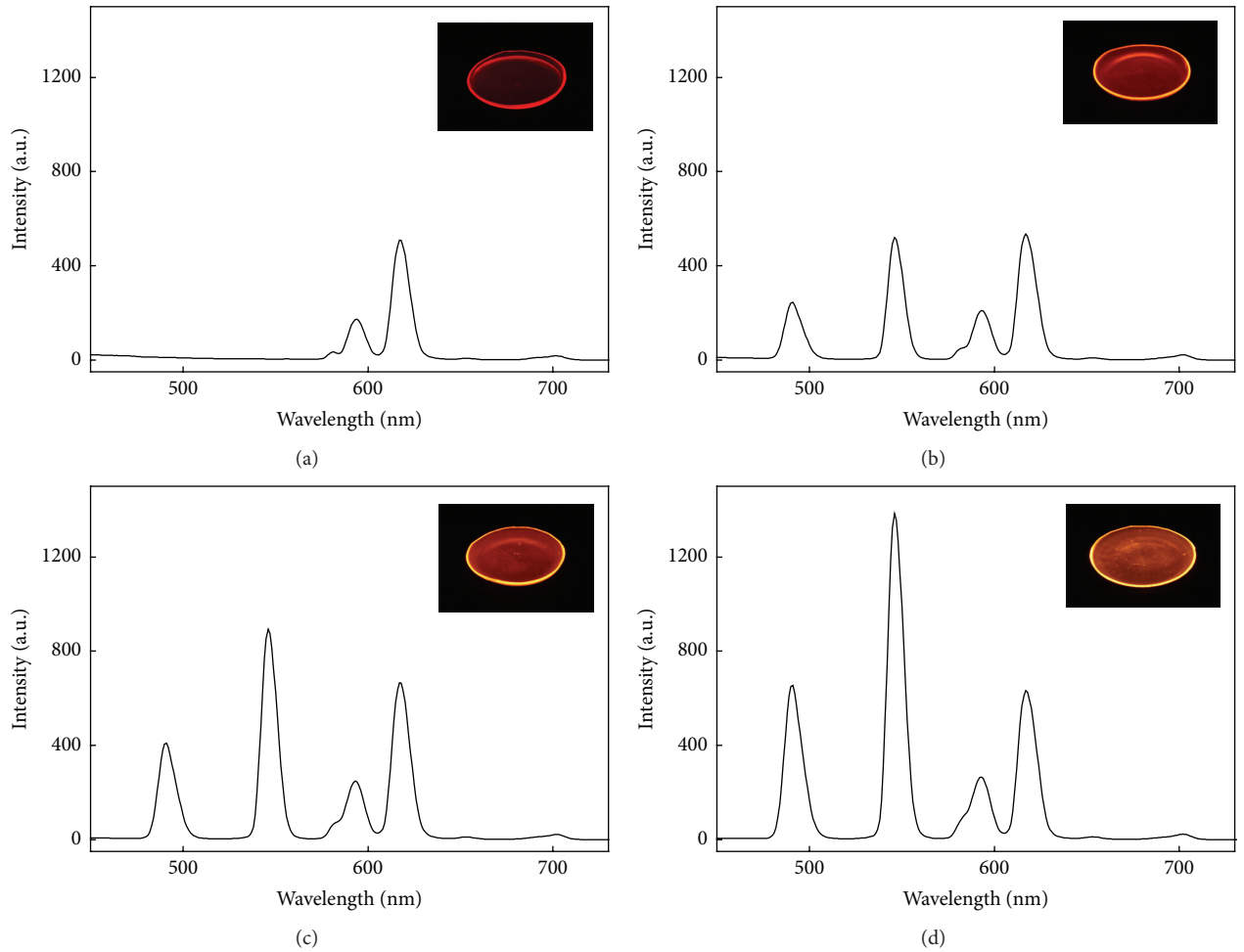

Figure 5: Emission spectra of (a) 0.2 wt% EBA, (b) 0.4 wt% TBA-0.2 wt% EBA, (c) 0.8 wt% TBA-0.2 wt% EBA, and (d) 1.4 wt% TBA-0.2 wt% EBA incorporated PMMA under 254 nm UV radiation. Inserted photos: fluorescence from corresponding samples.

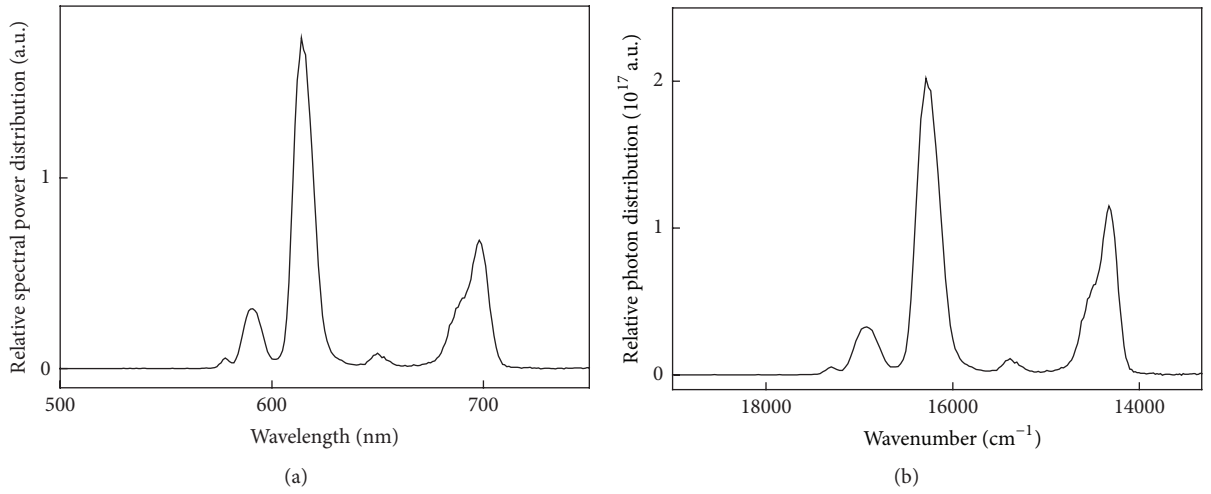

Figure 6: (a) Relative spectral power distribution and (b) relative photon distribution of 0.2 wt% EBA incorporated PMMA under 254 nm excitation.

Table 1: Relative photon numbers and number ratios in EBA incorporated PMMA.

Transition	Wave number (cm^{-1})	Relative photon number (10^{19} a.u.)	Relative photon number ratio
$^5D_0 \rightarrow {}^7F_1(N_1)$	16920	1.002	—
$^5D_0 \rightarrow {}^7F_2(N_2)$	16256	5.800	$N_2/N_1 = 5.79$
$^5D_0 \rightarrow {}^7F_4(N_4)$	14327	3.326	$N_4/N_1 = 3.32$

Table 2: Predicted spontaneous transition probabilities, branching ratios, and radiative lifetime of EBA incorporated PMMA.

Transition	$U^{(2)2}$	$U^{(4)2}$	$U^{(6)2}$	A_{ed} (s^{-1})	A_{md} (s^{-1})	A_T (s^{-1})	β (%)	τ_{rad} (ms)
$^5D_0 \rightarrow {}^7F_1$	0	0	0	0	56.44	570.88	9.89	1.75
$^5D_0 \rightarrow {}^7F_2$	0.0032	0	0	326.71	0		57.23	
$^5D_0 \rightarrow {}^7F_4$	0	0.0023	0	187.73	0		32.88	

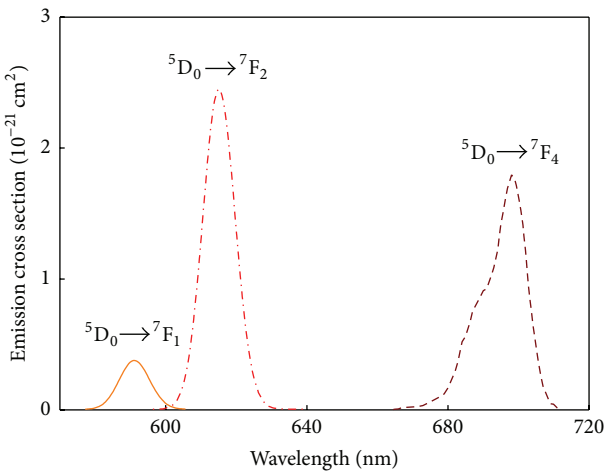

Figure 7: Emission cross section profiles of 0.2 wt% EBA incorporated PMMA.

fluorescence branching ratio β of the $^5D_0 \rightarrow {}^7F_2$ transition centered at 617 nm accounts for 57.23%, which is higher than those of other transitions, predicting that the $^5D_0 \rightarrow {}^7F_2$ transition emission is dominant among the transitions of Eu^{3+} in EBA incorporated PMMA.

To further evaluate the energy extraction efficiency for optical material, it is of great significance to discuss the emission cross section σ_e. The emission cross section for the transition emissions arising from $^5D_0$ level of Eu^{3+} reveals the radiative transition probabilities, which are determined through the Fuchtbauer-Ladenburg (FL) formula [69]:

$$\sigma_e = \frac{A_{rad}}{8\pi c n^2} \frac{\lambda^5 N(\lambda)}{\int \lambda N(\lambda)\, d\lambda}, \quad (8)$$

where n, A_{rad}, and $N(\lambda)$ represent the refractive index, spontaneous emission probability, and emission photon distribution, respectively. The σ_e profiles are shown in Figure 7 and the maximum values of σ_e for $^5D_0 \rightarrow {}^7F_J$ $(J = 1, 2, 4)$ transitions are deduced to be 0.377×10^{-21}, 2.451×10^{-21}, and 1.799×10^{-21} cm^2, respectively, and the large emission cross section enables the EBA incorporated PMMA to be a promising material for active optical devices.

Table 3: CIE chromaticity coordinates of the lanthanide complexes coincorporated PMMA.

Points in CIE diagram	EBA (wt%)	TBA (wt%)	x-coordinate	y-coordinate
1	0.2	0	0.6554	0.3397
2	0.2	0.4	0.6015	0.3816
3	0.2	0.8	0.5863	0.3967
4	0.2	1.4	0.5569	0.4200
5	0	0.2	0.3327	0.5877

The visible emission spectra of TBA/EBA coincorporated PMMA under 254 nm excitation are presented in Figure 5. With the introduction of TBA into EBA incorporated PMMA, seven strong and sharp emission bands are recorded under the same excitation condition. The 491 and 546 nm emission bands are attributed to the $^5D_4 \rightarrow {}^7F_6$ and $^5D_4 \rightarrow {}^7F_5$ characteristic transitions of Tb^{3+}, and the emission bands at 582, 593, and 617 nm are ascribed to the transitions from both Tb^{3+} and Eu^{3+} ions. Other bands peaking at 653 and 702 nm are typical emission features for the $^5D_0 \rightarrow {}^7F_J$ $(J = 3, 4)$ transitions of Eu^{3+} [60]. EBA single incorporated and TBA/EBA coincorporated PMMA samples exhibit various color fluorescence under the excitation of 254 nm UV radiation, as shown in the inserted photo of Figure 5. In order to exhibit the trace of color variation, the CIE color coordinates for EBA single incorporated and TBA/EBA coincorporated PMMA samples were calculated based on the relative spectral power distributions, as listed in Table 3. In the cases of a fixed concentration of EBA, the fluorescence color coordinates in CIE chromaticity diagram move along right boundary from the bottom to the top with the concentration of TBA varying from 0 to 1.4 wt%, as marked points 1, 2, 3, and 4 in Figure 4. The variation of color coordinates is originated from the superimposed effect of TBA and EBA, indicating that Ln complexes incorporated PMMA are a promising candidate for radiation conversion system and lighting device. Furthermore, intrinsic transition intensities of Eu^{3+} increase due to energy migration from Tb^{3+}, and the energy transfer process can be further exposed through the excitation behaviors [70, 71].

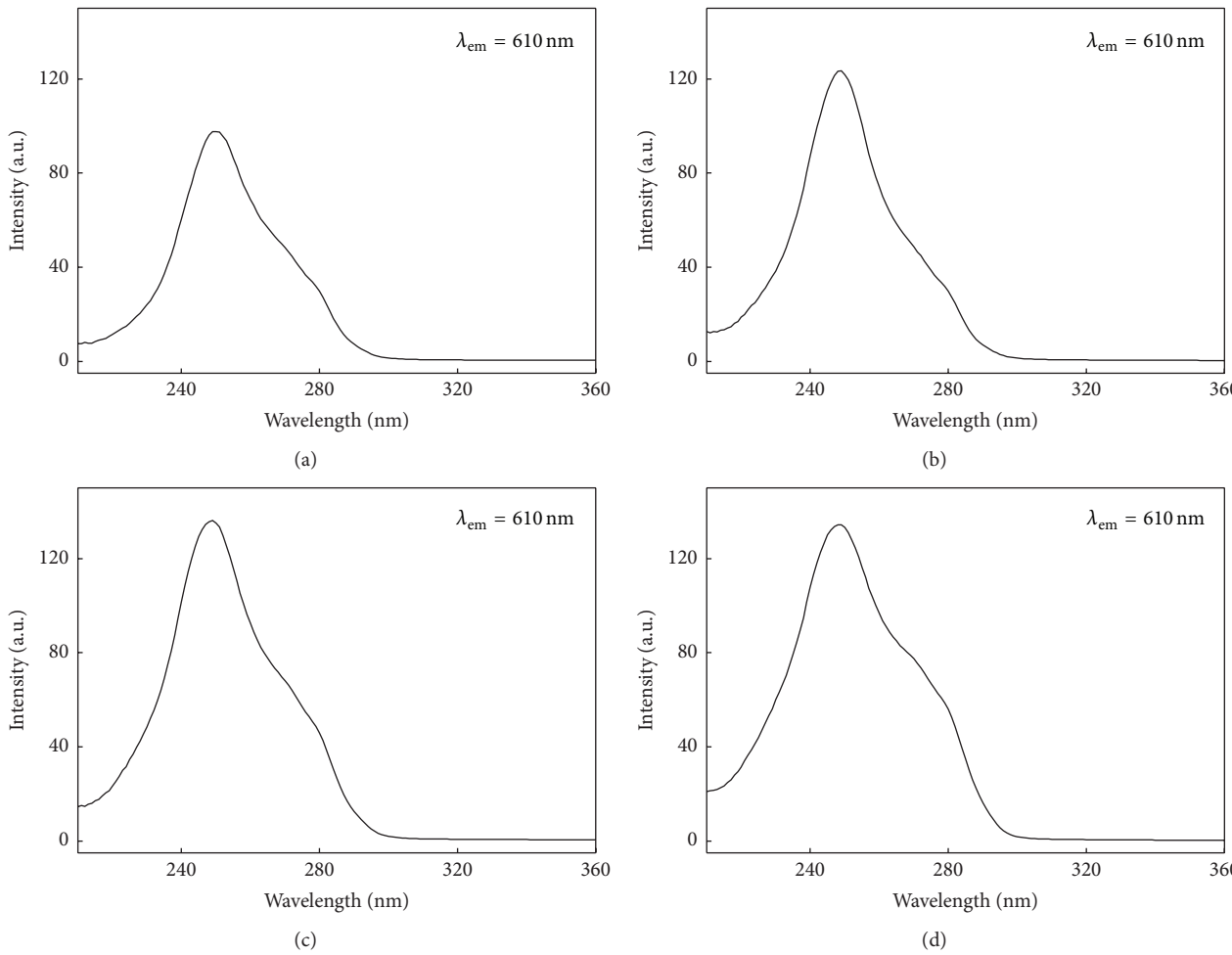

Figure 8: Excitation spectra of (a) 0.2 wt% EBA, (b) 0.4 wt% TBA-0.2 wt% EBA, (c) 0.8 wt% TBA-0.2 wt% EBA, and (d) 1.4 wt% TBA-0.2 wt% EBA incorporated PMMA.

In order to ascertain the occurrence of energy transfer between Tb^{3+} and Eu^{3+}, the excitation spectra are recorded by monitoring at 610 nm, which corresponds to $^5D_0 \rightarrow {}^7F_2$ emission transition of Eu^{3+}. It is comprised of a broad excitation band in the spectral region of 240–280 nm as presented in Figure 8, and the highest intensity is achieved in 0.8 wt% TBA-0.2 wt% EBA incorporated PMMA. The enhancement factor of 610 nm emissions between TBA/EBA coincorporated and EBA single incorporated PMMA under different excitation wavelengths has been derived from the excitation spectra, as shown in Figure 9. The enhancement factor is obviously larger than 1 when the excitation wavelength is located in 220–300 nm, which indicates that TBA/EBA coincorporated PMMA can be more efficiently excited by UV radiation compared with EBA single incorporated PMMA, especially in the short-wavelength UV region.

The luminescence mechanism of Ln complex incorporated PMMA is depicted in Figure 10. In EBA/TBA single incorporated PMMA, the Ln complex is excited from the singlet ground state S_0 to the singlet excited state S_1 by UV absorption first and then relaxes to the triplet state T_2 via intersystem crossing; after that an internal conversion $T_2 \rightarrow T_1$ takes place in triplet state. Subsequently, the energy is nonradiatively transferred from the triplet state of the ligands to the resonance state of the coordinated Tb^{3+} or Eu^{3+} [72–75]. Finally, the Tb^{3+} or Eu^{3+} emits visible characteristic fluorescence by the radiative transitions from the excited state to the ground states. Besides, in EBA/TBA coincorporated PMMA, a part of excitation energy in Tb^{3+} can be transferred to $^5D_3$ level of Eu^{3+} with the assistance of chemical bonds and then the excited Eu^{3+} transition radiatively to ^7F_J ($J = 0, 1, 2, 3, 4$) emitting visible light, which consequently bring about the enhanced visible fluorescence emission and improved photon conversion. Effective intramolecular and intermolecular energy transfers make TBA/EBA coincorporated PMMA promising for enhancement of lighting quality and conversion efficiency of solar cells employed in outer space.

4. Conclusions

Efficient green and red fluorescence is observed from terbium and europium benzoic acids (TBA and EBA) incorporated poly methyl methacrylate (PMMA) under ultraviolet (UV)

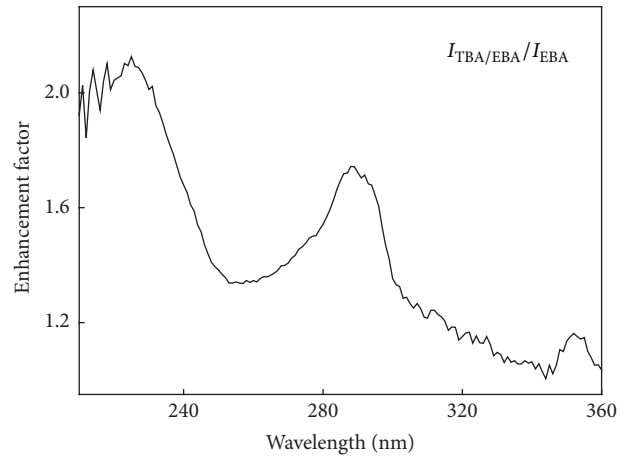

Figure 9: Enhancement factor of 610 nm fluorescence between 0.8 wt% TBA-0.2 wt% EBA coincorporated and 0.2 wt% EBA incorporated PMMA.

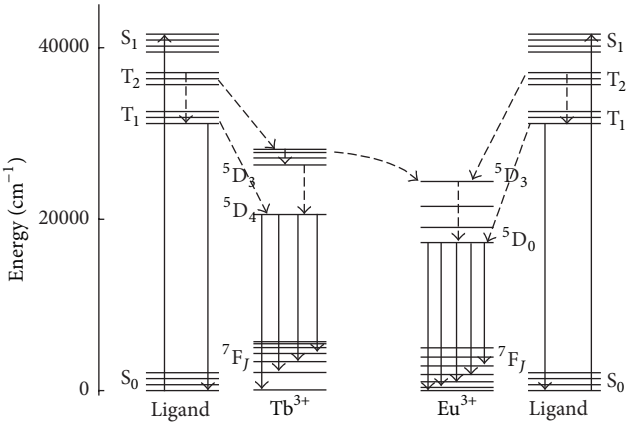

Figure 10: Schematic diagram of luminescence mechanism in TBA/EBA incorporated PMMA.

radiation. Judd-Ofelt intensity parameters Ω_2 and Ω_4 of EBA incorporated PMMA have been derived to be 11.13×10^{-20} and 13.15×10^{-20} cm^2, respectively, indicating a high inversion asymmetrical and strong covalent environment around Ln ions in PMMA. The maximum emission cross sections for $^5D_0 \rightarrow {}^7F_2$ transition in EBA incorporated PMMA are 2.451×10^{-21} cm^2, revealing the potential UV→Visible photons conversion capacity of Eu^{3+}. Color variation and fluorescence enhancement in TBA/EBA coincorporated PMMA are originated from superimposed effect of TBA and EBA. Furthermore, emission intensity of Eu^{3+} has been enhanced due to energy migration from Tb^{3+} with the assistant of chemical bonds. Effective photon conversion and superimposed effect in TBA/EBA coincorporated PMMA suggest that the Ln complexes incorporated PMMA is a potential candidate for lighting quality improvement and conversion efficiency increment of DSSCs.

Competing Interests

The authors declare that there are no competing interests regarding the publication of this paper and regarding the grants that they have received.

Acknowledgments

This work was supported by the National Natural Science Foundation of China (Grant no. 61275057).

References

[1] A. Yella, H.-W. Lee, H. N. Tsao et al., "Porphyrin-sensitized solar cells with cobalt (II/III)-based redox electrolyte exceed 12 percent efficiency," *Science*, vol. 334, no. 6056, pp. 629–634, 2011.

[2] S. H. Ko, D. Lee, H. W. Kang et al., "Nanoforest of hydrothermally grown hierarchical ZnO nanowires for a high efficiency dye-sensitized solar cell," *Nano Letters*, vol. 11, no. 2, pp. 666–671, 2011.

[3] J. Qi, W. Liu, C. Biswas et al., "Enhanced power conversion efficiency of CdS quantum dot sensitized solar cells with ZnO nanowire arrays as the photoanodes," *Optics Communications*, vol. 349, Article ID 20030, pp. 198–202, 2015.

[4] H. Choi, Y.-S. Chen, K. G. Stamplecoskie, and P. V. Kamat, "Boosting the photovoltage of dye-sensitized solar cells with thiolated gold nanoclusters," *The Journal of Physical Chemistry Letters*, vol. 6, no. 1, pp. 217–223, 2015.

[5] N. Yao, J. Huang, K. Fu et al., "Efficiency enhancement in dye-sensitized solar cells with down conversion material ZnO: Eu^{3+}, Dy^{3+}," *Journal of Power Sources*, vol. 267, pp. 405–410, 2014.

[6] S. Ivanova and F. Pellé, "Strong 1.53 μm to NIR-VIS-UV upconversion in Er-doped fluoride glass for high-efficiency solar cells," *Journal of the Optical Society of America B: Optical Physics*, vol. 26, no. 10, pp. 1930–1938, 2009.

[7] H. Hafez, M. Saif, and M. S. A. Abdel-Mottaleb, "Down-converting lanthanide doped TiO_2 photoelectrodes for efficiency enhancement of dye-sensitized solar cells," *Journal of Power Sources*, vol. 196, no. 13, pp. 5792–5796, 2011.

[8] L.-L. Li and E. W.-G. Diau, "Porphyrin-sensitized solar cells," *Chemical Society Reviews*, vol. 42, no. 1, pp. 291–304, 2013.

[9] T. Aguilar, J. Navas, D. M. De Los Santos et al., "TiO_2 and pyrochlore $Tm_2Ti_2O_7$ based semiconductor as a photoelectrode for dye-sensitized solar cells," *Journal of Physics D: Applied Physics*, vol. 48, no. 14, Article ID 145102, 2015.

[10] G. Katsagounos, E. Stathatos, N. B. Arabatzis, A. D. Keramidas, and P. Lianos, "Enhanced photon harvesting in silicon multicrystalline solar cells by new lanthanide complexes as light concentrators," *Journal of Luminescence*, vol. 131, no. 8, pp. 1776–1781, 2011.

[11] M. Sendova-Vassileva, "Model calculation of the effectiveness of Tb^{3+} containing glass as a wavelength converter in thin film solar cells," *Journal of Materials Science*, vol. 46, no. 22, pp. 7184–7190, 2011.

[12] V. D. Rodríguez, V. K. Tikhomirov, J. Méndez-Ramos, A. C. Yanes, and V. V. Moshchalkov, "Towards broad range and highly efficient down-conversion of solar spectrum by Er^{3+}-Yb^{3+} co-doped nano-structured glass-ceramics," *Solar Energy Materials and Solar Cells*, vol. 94, no. 10, pp. 1612–1617, 2010.

[13] V. Kumar, A. F. Khan, and S. Chawla, "Intense red-emitting multi-rare-earth doped nanoparticles of YVO_4 for spectrum

conversion towards improved energy harvesting by solar cells," *Journal of Physics D: Applied Physics*, vol. 46, no. 36, Article ID 365101, 2013.

[14] J. J. Velázquez, A. C. Yanes, J. del-Castillo, C. Guzmán-Afonso, and V. D. Rodríguez, "Dual emission in multiphase SiO_2–SnO_2–LaF_3 nanostructured glass-ceramics for simultaneous UV and NIR solar spectrum conversion," *Science of Advanced Materials*, vol. 7, no. 11, pp. 2272–2277, 2015.

[15] S. González-Pérez, J. Sanchiz, B. González-Díaz et al., "Luminescent polymeric film containing an Eu(III) complex acting as UV protector and down-converter for Si-based solar cells and modules," *Surface and Coatings Technology*, vol. 271, pp. 106–111, 2015.

[16] C.-Y. Sun, X.-J. Zheng, X.-B. Chen, L.-C. Li, and L.-P. Jin, "Assembly and upconversion luminescence of lanthanide-organic frameworks with mixed acid ligands," *Inorganica Chimica Acta*, vol. 362, no. 2, pp. 325–330, 2009.

[17] J. Lin, Q. Wang, C. Tan, and H. Chen, "Luminescence recognition behavior concerning different anions by lanthanide complex equipped with electron-withdraw groups and in PMMA matrix," *Synthetic Metals*, vol. 160, no. 15-16, pp. 1780–1786, 2010.

[18] G. Gheno, M. Bortoluzzi, R. Ganzerla, and F. Enrichi, "Inorganic pigments doped with tris(pyrazol-1-yl)borate lanthanide complexes: a photoluminescence study," *Journal of Luminescence*, vol. 145, pp. 963–969, 2014.

[19] C. K. Oliveira, V. P. de Souza, L. L. da Luz et al., "Synthesis, crystal structure and luminescent properties of lanthanide extended structure with asymmetrical dinuclear units based on 2-(methylthio)benzoic acid," *Journal of Luminescence*, vol. 170, pp. 528–537, 2016.

[20] A. M. Darwish, M. T. Sagapolutele, S. Sarkisov, D. Patel, D. Hui, and B. Koplitz, "Double beam pulsed laser deposition of composite films of poly(methyl methacrylate) and rare earth fluoride upconversion phosphors," *Composites Part B: Engineering*, vol. 55, pp. 139–146, 2013.

[21] S. Biju, Y. K. Eom, J.-C. G. Bünzli, and H. K. Kim, "A new tetrakis β-diketone ligand for NIR emitting Ln^{III} ions: luminescent doped PMMA films and flexible resins for advanced photonic applications," *The Journal of Materials Chemistry C*, vol. 1, no. 42, pp. 6935–6944, 2013.

[22] J. Zhang, W.-X. Li, B.-Y. Ao, S.-Y. Feng, and X.-D. Xin, "Fluorescence enhancement of europium(III) perchlorate by benzoic acid on bis(benzylsulfinyl)methane complex and its binding characteristics with the bovine serum albumin (BSA)," *Spectrochimica Acta Part A: Molecular and Biomolecular Spectroscopy*, vol. 118, pp. 972–980, 2014.

[23] F. Zinna, U. Giovanella, and L. D. Bari, "Highly circularly polarized electroluminescence from a chiral europium complex," *Advanced Materials*, vol. 17, pp. 1791–1795, 2015.

[24] R. Bonzanini, E. M. Girotto, M. C. Gonçalves, E. Radovanovic, E. C. Muniz, and A. F. Rubira, "Effects of europium (III) acetylacetonate doping on the miscibility and photoluminescent properties of polycarbonate and poly(methyl methacrylate) blends," *Polymer*, vol. 46, no. 1, pp. 253–259, 2005.

[25] D. S. Bodas, S. K. Mahapatra, and S. A. Gangal, "Comparative study of spin coated and sputtered PMMA as an etch mask material for silicon micromachining," *Sensors and Actuators, A: Physical*, vol. 120, no. 2, pp. 582–588, 2005.

[26] Y. A. Ustynyuk, N. E. Borisova, V. A. Babain et al., "N,N′-Dialkyl-N,N′-diaryl-1,10-phenanthroline-2,9-dicarboxamides as donor ligands for separation of rare earth elements with a high and unusual selectivity. DFT computational and experimental studies," *Chemical Communications*, vol. 51, no. 35, pp. 7466–7469, 2015.

[27] J. Zhang, L.-X. Wang, L. Zhang, Y. Chen, and Q.-T. Zhang, "Co-luminescence properties of terbium ions-benzoic acid-phen complexes doped with europium ions," *Rare Metals*, vol. 32, no. 6, pp. 599–604, 2013.

[28] Y. Wu, J. Wang, X. Kong et al., "A dinuclear europium(III) complex with thenoyltrifluoroacetonato and 1-(2-pyridylzao)-2-naphtholato ligands and its optical properties," *Inorganica Chimica Acta*, vol. 370, no. 1, pp. 346–352, 2011.

[29] B. Kokuoz, C. Kucera, J. R. DiMaio, and J. Ballato, "Organic-inorganic hybrid nanoparticles with enhanced rare-earth emissions," *Optical Materials*, vol. 31, no. 9, pp. 1327–1330, 2009.

[30] B. Yan and X.-F. Qiao, "Rare-earth/inorganic/organic polymeric hybrid materials: molecular assembly, regular microstructure and photoluminescence," *Journal of Physical Chemistry B*, vol. 111, no. 43, pp. 12362–12374, 2007.

[31] B. Gao, L. Chen, and T. Chen, "Effect of electron-donating substituent groups on aromatic ring on photoluminescence properties of complexes of benzoic acid-functionalized polysulfone with Eu(III) ions," *Physical Chemistry Chemical Physics*, vol. 17, no. 38, pp. 25322–25332, 2015.

[32] Q. Zhang, Y. Sheng, K. Zheng, X. Qin, P. Ma, and H. Zou, "Novel organic-inorganic amorphous photoactive hybrid films with rare earth (Eu^{3+}/s Tb^{3+}) covalently embedded into silicon-oxygen network via sol-gel process," *Materials Research Bulletin*, vol. 70, pp. 379–384, 2015.

[33] G. Sharma and A. K. Narula, "Effect of doping of calcium fluoride nanoparticles on the photoluminescence properties of europium complexes with benzoic acid derivatives as secondary ligands and 2-aminopyridine as primary ligand," *Optical Materials*, vol. 46, pp. 438–443, 2015.

[34] W. X. Wu, T. X. Wang, X. Wang et al., "Hybrid solar concentrator with zero self-absorption loss," *Solar Energy*, vol. 84, no. 12, pp. 2140–2145, 2010.

[35] Q. Ma, W. Yu, X. Dong, J. Wang, G. Liu, and J. Xu, "Electrospinning fabrication and properties of Fe_3O_4/Eu$(BA)_3$phen/PMMA magnetic-photoluminescent bifunctional composite nanoribbons," *Optical Materials*, vol. 35, no. 3, pp. 526–530, 2013.

[36] V. I. Gerasimova, A. A. Antoshkov, Y. S. Zavorotny, A. O. Rybaltovskii, and D. A. Lemenovskii, "Optical properties of europium(III) β-diketonate/polymer-doped systems using supercritical carbon dioxide," *Journal of Luminescence*, vol. 134, pp. 339–344, 2013.

[37] T. Monzón-Hierro, J. Sanchiz, S. González-Pérez et al., "A new cost-effective polymeric film containing an Eu(III) complex acting as UV protector and down-converter for Si-based solar cells and modules," *Solar Energy Materials and Solar Cells*, vol. 136, pp. 187–192, 2015.

[38] L. Liu, M. Yu, J. Zhang, B. Wang, W. Liu, and Y. Tang, "Facile fabrication of color-tunable and white light emitting nano-composite films based on layered rare-earth hydroxides," *Journal of Materials Chemistry C*, vol. 3, no. 10, pp. 2326–2333, 2015.

[39] S. Rodríguez, P. Elizondo, S. Bernès, N. Pérez, R. Bustos, and E. García-España, "Mechanochemical synthesis of an Eu(III) complex. Preparation and Luminescence Properties of PMMA:[$C_{42}H_{38}N_5O_{19}$Eu] Hybrid Films," *Polyhedron*, vol. 85, pp. 10–14, 2015.

[40] H. Jiu, J. Ding, Y. Sun, J. Bao, C. Gao, and Q. Zhang, "Fluorescence enhancement of europium complex co-doped

with terbium complex in a poly(methyl methacrylate) matrix," *Journal of Non-Crystalline Solids*, vol. 352, no. 3, pp. 197–202, 2006.

[41] Z. Zhang, C. Yu, L. Liu et al., "Efficient near-infrared (NIR) luminescent PMMA-supported hybrid materials doped with tris-β-diketonate Ln^{3+} complex (Ln = Nd or Yb)," *Journal of Photochemistry and Photobiology A: Chemistry*, vol. 314, pp. 104–113, 2016.

[42] H. Q. Gu, Y. J. Hou, F. Xu, and S. H. Wang, "Electrospinning preparation, thermal, and luminescence properties of $Eu_2(BTP)_3(Phen)_2$ complex doped in PMMA," *Colloid and Polymer Science*, vol. 293, no. 8, pp. 2201–2208, 2015.

[43] R. Puthiyottil, S. Varghese, U. Gopalakrishnapanicker, and J. T. Guthrie, "Characterization of europium complex-doped PMMA and PMMA-EVA polymer networks," *Polymer—Plastics Technology and Engineering*, vol. 53, no. 11, pp. 1111–1118, 2014.

[44] A. K. Singh, S. K. Singh, H. Mishra, R. Prakash, and S. B. Rai, "Structural, thermal, and fluorescence properties of $Eu(DBM)_3$Phenx complex doped in PMMA," *Journal of Physical Chemistry B*, vol. 114, no. 41, pp. 13042–13051, 2010.

[45] H. Jiu, L. Zhang, G. Liu, and T. Fan, "Fluorescence enhancement of samarium complex co-doped with terbium complex in a poly(methyl methacrylate) matrix," *Journal of Luminescence*, vol. 129, no. 3, pp. 317–319, 2009.

[46] J. Garcia-Torres, P. Bosch-Jimenez, E. Torralba-Calleja et al., "Highly efficient luminescent materials: influence of the matrix on the photophysical properties of Eu(III) complex/polymer hybrids," *Journal of Photochemistry and Photobiology A: Chemistry*, vol. 283, pp. 8–16, 2014.

[47] M. S. Attia, A. M. Othman, A. O. Youssef, and E. El-Raghi, "Excited state interaction between hydrochlorothiazide and europium ion in PMMA polymer and its application as optical sensor for hydrochlorothiazide in tablet and serum samples," *Journal of Luminescence*, vol. 132, no. 8, pp. 2049–2053, 2012.

[48] H.-G. Liu, X.-S. Feng, K. Jang et al., "Influences of compositions and ligands on photoluminescent properties of Eu(III) ions in composite europium complex/PMMA systems," *Journal of Luminescence*, vol. 127, no. 2, pp. 307–315, 2007.

[49] K. Buczko and M. Karbowiak, "Colour-tuneable double-layer polymeric films doped with lanthanide β-diketonate complexes," *Journal of Luminescence*, vol. 143, pp. 241–253, 2013.

[50] R. Puthiyottil, S. Varghese, U. Gopalakrishnapanicker, and J. T. Guthrie, "Optical properties of europium (2,2′-bipyridine-N,N-dioxide)$_2$ $(NO_3)_3$ complex-doped poly(methyl methacrylate)," *Polymer Engineering and Science*, vol. 53, no. 1, pp. 119–124, 2013.

[51] M. Bortoluzzi, G. Paolucci, M. Gatto et al., "Preparation of photoluminescent PMMA doped with tris(pyrazol-1-yl)borate lanthanide complexes," *Journal of Luminescence*, vol. 132, no. 9, pp. 2378–2384, 2012.

[52] T. Liu, G. Duan, Y. Zhang, J. Fang, and Z. Zeng, "Synthesis and characterization of the luminescent lanthanide complexes with two similar benzoic acids," *Spectrochimica Acta—Part A: Molecular and Biomolecular Spectroscopy*, vol. 74, no. 4, pp. 843–848, 2009.

[53] E. B. Gibelli, J. Kai, E. E. S. Teotonio, O. L. Malta, M. C. F. C. Felinto, and H. F. Brito, "Photoluminescent PMMA polymer films doped with Eu^{3+}-β-diketonate crown ether complex," *Journal of Photochemistry and Photobiology A: Chemistry*, vol. 251, pp. 154–159, 2013.

[54] B. Yue, Y.-N. Chen, H.-B. Chu, Y.-R. Qu, A.-L. Wang, and Y.-L. Zhao, "Synthesis, crystal structures and fluorescence properties of dinuclear Tb(III) and Sm(III) complexes with 2,4,6-tri(2-pyridyl)-1,3,5-triazine and halogenated benzoic acid," *Inorganica Chimica Acta*, vol. 414, pp. 39–45, 2014.

[55] H. Zhang, H. Song, B. Dong et al., "Electrospinning preparation and luminescence properties of europium complex/polymer composite fibers," *Journal of Physical Chemistry C*, vol. 112, no. 25, pp. 9155–9162, 2008.

[56] F. H. Walters, "Design of corrosion inhibitors: use of the hard and soft acid-base (HSAB) theory," *Journal of Chemical Education*, vol. 68, no. 1, pp. 29–31, 1991.

[57] H. Zhang, H. Dai, Y. Liu, J. Deng, L. Zhang, and K. Ji, "Surfactant-mediated PMMA-templating fabrication and characterization of three-dimensionally ordered macroporous Eu_2O_3 and Sm_2O_3 with mesoporous walls," *Materials Chemistry and Physics*, vol. 129, no. 1-2, pp. 586–593, 2011.

[58] Y. Hasegawa, H. Kawai, K. Nakamura, N. Yasuda, Y. Wada, and S. Yanagida, "Molecular design of luminescent Eu(III) complexes as lanthanide lasing material and their optical properties," *Journal of Alloys and Compounds*, vol. 408–412, pp. 669–674, 2006.

[59] H. Boubekri, M. Diaf, K. Labbaci, L. Guerbous, T. Duvaut, and J. P. Jouart, "Synthesis and optical properties of Tb^{3+} doped CdF_2 single crystals," *Journal of Alloys and Compounds*, vol. 575, pp. 339–343, 2013.

[60] V. Naresh and S. Buddhudu, "Energy transfer based enhanced red emission intensity from (Eu^{3+}, Tb^{3+}):LFBCd optical glasses," *Journal of Luminescence*, vol. 137, pp. 15–21, 2013.

[61] L. Mei, J. Xie, H. Liu, L. Liao, Y. Zhang, and M. Li, "Luminescence properties and energy transfer of Ce^{3+}/Tb^{3+} co-doped $Ca9La(PO4)_5(SiO_4)F_2$ phosphor," *Optics Communications*, vol. 335, pp. 90–93, 2015.

[62] J. Guan, B. Chen, Y. Sun, H. Liang, and Q. Zhang, "Effects of synergetic ligands on the thermal and radiative properties of $Eu(TTA)_3nL$-doped poly(methyl methacrylate)," *Journal of Non-Crystalline Solids*, vol. 351, no. 10-11, pp. 849–855, 2005.

[63] M. P. Hehlen, M. G. Brik, and K. W. Krämer, "50th anniversary of the Judd-Ofelt theory: an experimentalist's view of the formalism and its application," *Journal of Luminescence*, vol. 136, pp. 221–239, 2013.

[64] Y. Liu, D. Tu, H. Zhu, and X. Chen, "Lanthanide-doped luminescent nanoprobes: controlled synthesis, optical spectroscopy, and bioapplications," *Chemical Society Reviews*, vol. 42, no. 16, pp. 6924–6958, 2013.

[65] C. E. Secu, D. Predoi, M. Secu, M. Cernea, and G. Aldica, "Structural investigations of sol-gel derived silicate gels using Eu^{3+} ion-probe luminescence," *Optical Materials*, vol. 31, no. 11, pp. 1745–1748, 2009.

[66] Y. Gandhi, I. V. Kityk, M. G. Brik, P. R. Rao, and N. Veeraiah, "Influence of tungsten on the emission features of Nd^{3+}, Sm^{3+} and Eu^{3+} ions in ZnF_2-WO_3-TeO2 glasses," *Journal of Alloys and Compounds*, vol. 508, no. 2, pp. 278–291, 2010.

[67] R. T. Moura Jr., A. N. Carneiro Neto, R. L. Longo, and O. L. Malta, "On the calculation and interpretation of covalency in the intensity parameters of $4f$-$4f$ transitions in Eu^{3+} complexes based on the chemical bond overlap polarizability," *Journal of Luminescence*, vol. 170, part 2, pp. 420–430, 2016.

[68] M. Dejneka, E. Snitzer, and R. E. Riman, "Blue, green and red fluorescence and energy transfer of Eu^{3+} in fluoride glasses," *Journal of Luminescence*, vol. 65, no. 5, pp. 227–245, 1995.

[69] V. Naresh, B. H. Rudramadevi, and S. Buddhudu, "Cross-relaxations and non-radiative energy transfer from (^{4}G5/2)

Sm^{3+} →(5D0) Eu^{3+}: B_2O_3-ZnO glasses," *Journal of Alloys and Compounds*, vol. 632, pp. 59–67, 2015.

[70] N. T. Kalyani, S. J. Dhoble, and R. B. Pode, "Enhancement of photoluminescence in various $Eu_xRe_{(1-x)}TTA_3Phen$ (Re = Y, Tb) complexes molecularly doped in PMMA," *Indian Journal of Physics*, vol. 86, no. 7, pp. 613–618, 2012.

[71] Y. Luo, Q. Yan, S. Wu, W. Wu, and Q. Zhang, "Inter- and intra-molecular energy transfer during sensitization of $Eu(DBM)_3Phen$ luminescence by $Tb(DBM)_3Phen$ in PMMA," *Journal of Photochemistry and Photobiology A: Chemistry*, vol. 191, no. 2-3, pp. 91–96, 2007.

[72] A. de Bettencourt-Dias and S. Viswanathan, "Nitro-functionalization and luminescence quantum yield of Eu(III) and Tb(III) benzoic acid complexes," *Dalton Transactions*, vol. 34, pp. 4093–4103, 2006.

[73] Y. H. Kim, N. S. Baek, and H. K. Kim, "Sensitized emission of luminescent lanthanide complexes based on 4-naphthalen-1-yl-benzoic acid derivatives by a charge-transfer process," *ChemPhysChem*, vol. 7, no. 1, pp. 213–221, 2006.

[74] S. Lis, M. Elbanowski, B. Makowska, and Z. Hnatejko, "Energy transfer in solution of lanthanide complexes," *Journal of Photochemistry and Photobiology A: Chemistry*, vol. 150, no. 1–3, pp. 233–247, 2002.

[75] K. Lun, Q. L. Ma, M. Yang et al., "Electricity-magnetism and color-tunable trifunction simultaneously assembled into one strip of flexible microbelt via electrospinning," *Chemical Engineering Journal*, vol. 279, pp. 231–240, 2015.